Indian Journal of Pure & Applied Physics
Vol. 63, January 2025, pp. 9-21
DOI: 10.56042/ijpap.v63i1.9124

A New Threshold Voltage Model of Short Channel FD-SOI MOSFET by Green's Function Approach to Analytically Solving 2-D Laplace/Poisson's Equations in Multi-Zone Structure and Applying it to Study Post-Implant Annealing Effect

Krishna Meel[a*], Ram Gopal[b] & Chitra Gautam[c]

[a]Department of physics, BK. Birla Institute of Engineering and Technology, Pilani (Rajasthan)-333 031, India

[b]Smart Sensors Group, CSIR-Central Electronics Engineering Research Institute, Pilani (Rajasthan)-333 031, India

[c]Acoustics and Vibration Metrology, Physico-Mechanical Metrology Division,
CSIR-National Physical Laboratory (CSIR-NPL), Delhi-110 012, India

Received 27 February 2024; accepted 17 December 2024

This paper reports on new analytical models of front and back gate threshold voltages for short-channel fully depleted silicon-on-insulator (FD-SOI) MOSFETs, considering an annealed non-uniform impurity profile resulting from retrograde doping required for vertical channel engineering. For this purpose, the exact solutions of multi-zone 2-D Laplace/Poisson equations have been obtained by adopting a new Green's function approach. Since the SOI MOSFET is a three-layer structure, we have established new multi-zone Green's functions that incorporate the combined effects of all three layers joined together at the interfaces. This approach allows for a more nuanced analysis of potential distributions in the three-layer structure of SOI devices, taking into account the interactions between the different layers within the device. Considering the explicit potential relations thus derived, we formulate closed-form expressions of front and back gate threshold voltages, which include the front and back gate charge coupling effects, the profile annealing effect, and the effects of drain and gate voltages. This holistic perspective is crucial because it enables a more accurate understanding of how these variables interact and affect device operation, thereby enhancing the predictive capability of the models. In addition to the front and back gate threshold voltages, their biasing counterparts—the respective back and front gate voltages—have also been formulated, accounting for the aforementioned effects, in order to determine operational modes of the device under study. Finally, the results obtained from the new model have been rigorously validated by comparison with data generated by ATLAS software, revealing excellent alignment between the two. This validation not only supports the reliability of the proposed models but also enhances their applicability in practical semiconductor device simulation and design.

Keywords: FD-SOI MOSFET's; Retrograde doping; Channel Engineering; Threshold voltage model; Annealing effect; Green's function approach

1 Introduction

The advancement in technology and device engineering has led to a considerable reduction in the size of MOSFETs, improving device response times and enhancing gate control capabilities. However, these developments have also resulted in significant short-channel effects that cannot be overlooked. To mitigate short-channel effects, various device structures have been proposed, such as FinFETs, Gate-All-Around (GAA) MOSFETs, and Multiple Gate FETs. This evolution has facilitated numerous applications of MOSFETs across diverse fields; for instance, biosensors based on FET[1-5] technology have garnered substantial attention in recent years. Additionally, MOSFETs exhibit high potential for high-frequency analog and RF applications[6]. The diverse research and application landscape of MOSFETs highlights the potential for future advancements. As the demand for smaller, faster, and more efficient electronic devices continues to grow, ongoing innovations in MOSFET technology, including novel materials, structures, and fabrication techniques, will play a crucial role in addressing emerging challenges and expanding their applications.

Fully-depleted (FD) enhancement mode MOSFET's fabricated on ultra-thin silicon-on-insulator (SOI) film attracted considerable attention from researchers due to their superior immunity from short-channel effects and improved sub-threshold swing compared to bulk MOSFETs. Because of these merits, SOI MOSFET's have turned out to be high speed and low power circuit elements for future VLSI application. For VLSI

*Corresponding author: (E-mail: krishna.meel@gmail.com)

circuits, miniaturization of SOI MOSFET device has been a general trend of technology development. However, scaling down of device channel length induces the short channel effect thereby deteriorating its characteristics[7-8].Due to sensitivity of short channel SOI MOSFET to the process fluctuations, the device design to meet the required specifications becomes very difficult; however this problem can be addressed through accurate analysis of the device behavior.

The process of retrograde doping by ion implantation has widely been used for vertical channel engineering of SOI MOSFET's[9-10] in order to minimize the short channel effect and to adjust the threshold voltage. In this process, just after implantation, the annealing is performed to eliminate the defects generated during the implantation. Although the original implant redistributes during the heat treatment, the annealed impurity profile still resembles with Gaussian distribution[11-14] that is vertical to channel length and along the channel it becomes almost uniform. Therefore, such non-uniform channel doping, including the annealing effect, must be considered for an accurate analysis of SOI MOSFETs.

Accounting for non-uniform doping, Pandey *et al.*[15] proposed a threshold voltage model for short channel SOI MESFET. This model solved 2-D Poisson's equations considering parabolic trial function of potential within SOI film. Such an assumption underestimates the effects of source and drain junctions that may cause erroneous results when the channel of the device is very short. Moreover, the doping profile considered in their analysis did not include the annealing effect. Thereafter, Zhang and co-workers[16]reported a short channel threshold voltage model by taking into account the non-uniform impurity profile in the channel region of SOI MOSFET. In this model, 2-D Laplace/Poisson's equations were solved by assuming a parabolic trial function of potential in buried oxide and a linear trial function coupled with a doubly integrated Gaussian profile in SOI film. However, the enforcement of such oversimplified solutions may give rise to erroneous results when the channel is very short. Furthermore, the model could not include the annealing effect in the doping profile.

To analytically solve 2-D Poisson's equation, the appropriate boundary conditions and suitable solution methods are necessary to predict the accurate behavior of the short channel SOI MOSFET. The most trusted method is Green's function technique which gives the exact solution of 2-D Poisson's equation including non-uniform channel doping profile. This technique was first employed for solving 2-D Poisson's equation to study short channel bulk MOSFET by Lin and Wu[17]. Later, Chin and Wu[18] and Guo and Wu[19] used the multi-zone Green's functions to analyze uniformly doped short gate MESFET and short channel SOI MOSFET respectively. In the year 2001, this method was also followed by Meer *et al.*[71] to study short channel SOI MOSFET with halos or pockets in SOI film.

However, the application of independent-zone Green's functions in the aforesaid analyses[18-20] is doubtable, because these functions were derived by considering their gradients normal to interfaces zero thereby rendering the Green's functions of each zone independent of the conditions at the other. These Green's functions consist of only geometrical parameters of individual zones but not the material properties, so they seem to be the mirror effects of each other. As a result, the solution of Laplace/Poisson's equations in multi-zone structure, by using these Green's functions under the conditions of field refraction at the interfaces, does not describe the real situation. Consequently, new Green's functions for multi-zone structures need to be established by carefully choosing the appropriate boundary conditions at the interfaces as these conditions directly transfer into the final solutions.

Our objective in this paper is to report a new analytical model of threshold voltages for short channel FD-SOI MOSFET's with non-uniform channel doping that incorporates the annealing effect. For this purpose we have solved Poisson's equation in depleted SOI film and Laplace equation in both front and back oxide layer of MOSFET to achieve the explicit 2-D potential relations in all the three layers. This has been carried out by using the rigorous Green's function technique. Since the SOI MOSFET is a three-layer structure, we have established new Green's functions for multi-zone media, and the procedure followed to obtain these functions is the most general. Considering the potential relations thus obtained, we have formulated both front and back gate threshold voltages by taking into account the charge coupling at both interfaces. Besides, their counterparts, the respective back and front gate biases, have also been formulated to determine the operational modes of the device. Finally, we have

validated the present model by comparing it with ATLAS data, showing excellent agreement between the two.

2 Mathematical Model

Figure 1(a) is the schematic representation of the fully depleted SOI MOSFET used in the present analysis and simulation. The y- and z-axis are oriented along and vertical to the front silicon-oxide interface, respectively. The origin, O(0,0), of y, and z coordinates is located at the midpoint of the front gate oxide-silicon interface. The source end exists at $y = -L/2$, while, that opposite to this at $y = L/2$ is the drain end, where L is the channel length. The thickness of the front gate oxide is t_{ox}, the thickness of buried oxide is t_{box} and that of the SOI film is t_{si}. In the case of the fully depleted SOI film with non-uniform doping influenced by the annealing effect, the 2-D Laplace equations in front and back oxide regions, as well as Poisson's equation in the SOI film under electrostatic conditions for n-channel MOSFET, can be expressed as follows:

$$\nabla^2 \phi_{ox} = 0, \quad \text{... (1)}$$

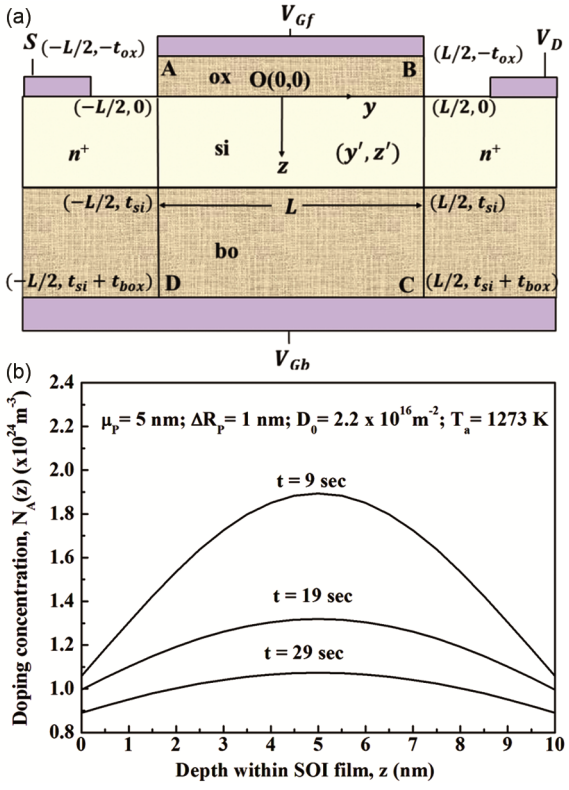

Fig. 1 — (a) 2-D Schematic view of SOI MOSFET (b) annealing effect on doping concentration within SOI film for different annealing time, t

$$\nabla^2 \phi_{si} = \frac{qN_A(z)}{\varepsilon_0 \varepsilon_{si}}, \quad \text{... (2)}$$

$$\nabla^2 \phi_{bo} = 0. \quad \text{... (3)}$$

Here, ε_0 is the vacuum dielectric constant, ε_{si} is the relative permittivity of silicon, q is the electronic charge and $N_A(z)$represents the implanted acceptor impurity after heat treatment. Assuming that there is no difference of projection range,R_p, between oxide and silicon, the impurity profile immediately after the implantation into the SOI film, which has a uniform base concentration, C_B, follows the Gaussian distribution given by[11]

$$N_A(z) = \frac{D_0}{\sqrt{2\pi}(\Delta R_p)} \exp\left\{-\frac{1}{2}\left(\frac{z-R_p+t_{ox}}{\Delta R_p}\right)^2\right\} + C_B, \quad \text{... (4)}$$

where D_0 is the ion implantation dose and ΔR_p is the standard deviation of ions. After annealing at temperatureT_a for time$t$, the standard deviation is assumed to be root mean square of ΔR_p and $\sqrt{2Dt}$, whereby the impurity redistribution occurs and the profile in Eq. (4) takes the form[21]:

$$N_A(z) = \frac{D_0}{\sqrt{2\pi}\sigma_P} \exp\left\{-\frac{1}{2}\left(\frac{z-\mu_p}{\sigma_p}\right)^2\right\} + C_B, \quad \text{... (5)}$$

Where

$$\mu_p = R_p - t_{ox},$$

$$\sigma_p^2 = \left(\Delta R_p\right)^2 + 2Dt,$$

Here, D is the impurity diffusion constant, which for boron is given by[22]

$$D = 2.1 \times 10^{-3} \exp\left(-\frac{2.85q}{kT_a}\right) (\text{cm}^2/\text{s}).$$

Here,k is the Boltzmann constant. The impurity profile in Eq. (5), with negligibly small base doping,C_B,compared to the implanted concentration, is used in the Poisson's Eq. (2) for the analysis of the present device. The depth profile of boron within SOI film for different annealing times at temperature 1133 K is shown in Fig. 1(b). This indicates that the impurity concentration decreases as the annealing time increases, with this effect more pronounced at the peak concentration. Here we neglect mobile carriers in Poisson's equation for convenient solution of the same. We justify this neglect later in the next section.The boundary conditions assumed for solving Eqs. (1)-(3) are given as follows[19,23]:

$$\phi_{ox}(y, z = -t_{ox}) = V'_{Gf}, \quad \text{... (6)}$$

$$\phi_{ox}(-L/2\,, z) = \frac{\phi_{SS}^{f} - V'_{Gf}}{t_{ox}} z + \phi_{SS}^{f}, \quad \text{... (7)}$$

$$\phi_{si}(-L/2\,, z) = V_{bi}(z), \quad \text{... (8)}$$

$$\phi_{bo}(-L/2\,, z) = \frac{V'_{Gb} - \phi_{SS}^{b}}{t_{box}}(z - t_{si}) + \phi_{SS}^{b}, \quad \text{... (9)}$$

$V'_{Gf} = V_{Gf} - V_{FB}^{f}$, at the front gate and source end, while those at the drain end and at back gate are

$$\phi_{ox}(L/2\,, z) = \frac{\phi_{SS}^{f} + V_D - V'_{Gf}}{t_{ox}} z + \phi_{SS}^{f} + V_D, \quad \text{... (10)}$$

$$\phi_{si}(L/2\,, z) = V_{bi}(z) + V_D, \quad \text{... (11)}$$

$$\phi_{bo}(L/2\,, z) = \frac{V'_{Gb} - \phi_{SS}^{b} - V_D}{t_{box}}(z - t_{si}) + \phi_{SS}^{b} + V_D, \quad \text{... (12)}$$

$$\phi_{bo}(y, z = t_{si} + t_{box}) = V'_{Gb} \quad \text{... (13)}$$

$V'_{Gb} = V_{Gb} - V_{FB}^{b}$.

Now, the boundary conditions for front oxide-silicon interface and back oxide-silicon interface can be written as

$$\phi_{ox}(y, z = 0\,) = \phi_{si}(y, z = 0\,), \quad \text{... (14)}$$

$$\frac{\partial \phi_{ox}}{\partial z}(y, z = 0\,) = \eta \frac{\partial \phi_{si}}{\partial z}(y, z = 0\,), \quad \text{.... (15)}$$

$$\phi_{si}(y, z = t_{si}) = \phi_{bo}(y, z = t_{si}), \quad \text{... (16)}$$

$$\eta \frac{\partial \phi_{si}}{\partial z}(y, z = t_{si}) = \frac{\partial \phi_{bo}}{\partial z}(y, z = t_{si}) \quad \text{.... (17)}$$

Here, $\eta = \varepsilon_{si}/\varepsilon_{ox}$, ε_{ox} is the relative permittivity of oxide, V_{Gf} is the front gate voltage, V_{Gb} is the back gate bias, $V_{FB}^{f,b}$ are the front and back gate flat-band voltages respectively. For n^+-p source and drain junctions, the built-in potential, $V_{bi}(z) = E_g/2 + (kT/q)\ln\{N_A(z)/n_i\}$, is the function of z due to non-uniform doping. Other parameters are: n_i −intrinsic concentration, E_g −energy band gap, V_D −source to drain applied voltage and T −absolute temperature. The front- and back-interface source end potential are $\phi_{SS}^{f} = V_{bi}(z = 0)$ and $\phi_{SS}^{b} = V_{bi}(z = t_{si})$ respectively. The boundary condition described by Eq. (13) assumes that the substrate below the buried oxide is highly doped(n^+), which means that the buried oxide substrate interface maintains an accumulation condition. As a resultV_{Gb} appears in toto at back oxide gate.

Recently, many researchers have addressed the 2-D Poission's equation in cylindrical coordinates by incorporating a parabolic potential profile[24-25] for biosensing application of MOSFETs. In order to solve the 2-D differential Eqs. (1)-(3), we employed a rigorous Green's function method. The process of establishing new multi-zone Green's functions, along with the approach used to derive explicit solutions of the aforementioned differential equations, is described below.

2.2 Green's functions and solutions

There is wide range of the problems in which Laplace's equations, together with Poisson's equation, are needed to be solved in multi-zone structure with three media joined at two interfaces, as illustrated in Fig. 1(a). Appropriately for 3-zone structure, we derive new Green's functions considering their basic definitions associated with Eqs. (1)-(3) subject to homogeneous conditions of boundary values given by Eqs. (6)-(13) at the outer boundaries, and real boundary conditions equivalent to Eqs. (14)-(17) at two interfaces instead of their zero normal derivative at the interfaces as has been done in the earlier publication[19]. Inspired from the work of Inglesfield[26], we shall now demonstrate that it is possible to directly find out the Green's function,$G(y, z; y', z')$, which represents the multi zones *en masse* joined on interfaces. As per active portion ABCD of Fig. 1(a), let us now keep the source point (y', z') fixed at silicon film and consider $G(y, z;\ y', z')$ as a function of y and z alone, which vary throughout the three-zone system, including the interfaces. Thus, the Green's function set representing silicon along with the effects of the adjoining layers (front oxide and buried oxide) is defined as:

$$\left.\begin{aligned} \nabla^2 G_{ox}^{si}(y, z;\ y', z') &= 0, \\ \nabla^2 G_{si}^{si}(y, z;\ y', z') &= \delta(y - y')\delta(z - z'), \\ \nabla^2 G_{bo}^{si}(y, z;\ y', z') &= 0. \end{aligned}\right\} \quad \text{... (18)}$$

Similarly, by assuming that the source point (y', z') is located in front oxide, the Green's functions, which include the effects of the other layers, are represented by the differential equations expressed as:

$$\left.\begin{aligned}\nabla^2 G_{ox}^{ox}(y,z;\,y',z') &= \delta(y-y')\delta(z-z'),\\ \nabla^2 G_{si}^{ox}(y,z;\,y',z') &= 0,\\ \nabla^2 G_{bo}^{ox}(y,z;\,y',z') &= 0,\end{aligned}\right\} \quad \text{... (19)}$$

and those in case when point (y', z') is kept fixed in buried oxide, are governed by

$$\left.\begin{aligned}\nabla^2 G_{ox}^{bo}(y,z;\,y',z') &= 0,\\ \nabla^2 G_{si}^{bo}(y,z;\,y',z') &= 0,\\ \nabla^2 G_{bo}^{bo}(y,z;\,y',z') &= \delta(y-y')\delta(z-z').\end{aligned}\right\} \quad \text{... (20)}$$

The subscripts in Green's functions indicate the respective regions, as such it is single function, $G(y,z;\,y',z')$, appeared in each of Eqs. (18)-(20). However, each set of differential equations pertains to the individual layer, incorporating combined effects from the other two layers based on the location of the source points indicated by the superscripts. In the conventional manner[27], we multiply Eqs. (1) to (3) by $G(y,z;\,y',z')$ and Eqs. (18) to (20) by ϕ and then subtract the latter from the former one. Thereafter, we apply the Green's theorem to yield:

$$\begin{aligned}\phi_{si} =& \frac{1}{\eta}\oint\left[\phi_{ox}\nabla G_{ox}^{si} - G_{ox}^{si}\nabla\phi_{ox}\right].dS\\ &+\frac{1}{\eta}\oint\left[\phi_{bo}\nabla G_{bo}^{si} - G_{bo}^{si}\nabla\phi_{bo}\right].dS\\ &+\oint\left[\phi_{si}\nabla G_{si}^{si} - G_{si}^{si}\nabla\phi_{si}\right].dS\\ &+\iint\frac{qN_A(z)}{\varepsilon_0\varepsilon_{si}}G_{si}^{si}(y',z';y,z)\,dy'dz' \qquad \text{... (21)}\end{aligned}$$

This expression represents the potential distribution in the silicon layer. The potentials for the front and buried oxide layers are given by:

$$\begin{aligned}\phi_{ox,bo} =& \oint\left[\phi_{ox}\nabla G_{ox}^{ox,bo} - G_{ox}^{ox,bo}\nabla\phi_{ox}\right].dS\\ &+\oint\left[\phi_{bo}\nabla G_{bo}^{ox,bo} - G_{bo}^{ox,bo}\nabla\phi_{bo}\right].dS\\ &+\eta\oint\left[\phi_{si}\nabla G_{si}^{ox,bo} - G_{si}^{ox,bo}\nabla\phi_{si}\right].dS\\ &+\eta\iint\frac{qN_A(z)}{\varepsilon_0\varepsilon_{si}}G_{si}^{ox,bo}(y',z';y,z)dy'dz' \qquad \text{... (22)}\end{aligned}$$

Thus, the present formalism can be extended to any number of media joined at the interfaces.

The Green's functions obtained by solving Eqs. (18)-(20) include the combined effects of front oxide, SOI film and buried oxide layers of the SOI MOSFET. The consideration of Eqs. (14)-(17) at the interface leads to the inclusion of material properties in Green's functions. Furthermore, there is no need to evaluate the first to third integrals of Eqs. (21) and (22) at the interfaces since these would cancel each other out; only the external boundary integrals in these equations need to be evaluated. If the interface trap densities are included in boundary values Eqs. (14)-(17), then the evaluation of the aforesaid integrals at the interfaces becomes mandatory and the present Green's functions are still valid for such a situation. The Green's functions appeared in the above integral equations, as per Appendix, for the silicon layer derived from set of Eq. (18) are written as:

$$G_{ox}^{si}(y,z;y',z') = \frac{2}{\mathcal{T}_{sc}}\eta\sum_{n=1}^{\infty}g_n(y,y')\frac{f_{si}^{(n)}(z')f_{ox}^{(n)}(z)}{\Delta_n}, \quad \text{... (23a)}$$

$$G_{si}^{si}(y,z;y',z') = \frac{2}{\mathcal{T}_{sc}}\sum_{n=1}^{\infty}g_n(y,y')\frac{f_{si}^{(n)}(z')f_{si}^{(n)}(z)}{\Delta_n}, \quad \text{... (23b)}$$

$$G_{bo}^{si}(y,z;y',z') = \frac{2}{\mathcal{T}_{sc}}\eta\sum_{n=1}^{\infty}g_n(y,y')\frac{f_{si}^{(n)}(z')f_{bo}^{(n)}(z)}{\Delta_n}, \quad \text{... (23c)}$$

where

$$g_n(y,y') = \frac{\sinh\alpha_n(y'+L/2)\sinh\alpha_n(y-L/2)}{\alpha_n\sinh(\alpha_n L)};\ y>y'$$

$$g_n(y,y') = \frac{\sinh\alpha_n(y'-L/2)\sinh\alpha_n(y+L/2)}{\alpha_n\sinh(\alpha_n L)};\ y<y'$$

The Green's functions, G_{ox}^{ox}, G_{si}^{ox} and G_{bo}^{ox} corresponding to set Eq. (19) can be obtained merely by replacing the common Eigen function $f_{si}^{(n)}(z')$ of respective expressions in Eq. (23) by $f_{ox}^{(n)}(z')$ related to oxide zone. Here we have omitted the arguments of Green's function for brevity. Similarly, the replacement of $f_{si}^{(n)}(z')$ of respective Eq. (23) by Eigen function, $f_{bo}^{(n)}(z')$ related to buried oxide, leads to the set of Green's functions, G_{ox}^{bo}, G_{si}^{bo} and G_{bo}^{bo} representing the solutions of Eq. (20).

The use of Green's functions, Eq. (23) in evaluating integral Eq. (21) will yield the potential distribution in silicon film only, because the common Eigen function $f_{si}^{(n)}(z')$ belongs to that region. The second set of Green's functions, G_{ox}^{ox}, G_{si}^{ox} and G_{bo}^{ox}, consists of the common Eigen function, $f_{ox}^{(n)}(z')$, as a result, the integral Eq. (22) with the help of this set delivers the solution that corresponds to the front

oxide. On the other hand, the application of third Green's function set,G_{ox}^{bo},G_{si}^{bo} and G_{bo}^{bo}, on Eq. (22) yields the potential relation corresponding to the buried oxide. Thus, using the Green's functions and integral equations (21) and (22), along with boundary conditions provided by Eqs. (6)-(17), the solutions for Eqs. (1)-(3) in the respective SOI film, front oxide, and buried oxide layers can be expressed as:

$$\phi_{si} = V_{Gf}^{'} + \left(\frac{z+t_g}{\mathcal{T}_{sc}}\right)\left[V_{Gb}^{'} - V_{Gf}^{'} - \Psi_F\right]$$

$$+V_0\left[\left(\frac{z-\mu_p}{\sqrt{2}\sigma_p}\right)\mathrm{Er}(z) + \frac{1}{\sqrt{\pi}}\mathrm{Ex}(z)\right]$$

$$+\frac{2}{\mathcal{T}_{sc}}\sum_{n=1}^{\infty}\frac{f_{si}^{(n)}(z)}{\alpha_n\Delta_n}F_n\left(V_{Gf}^{'}, V_{Gb}^{'}; y\right), \quad \text{... (24)}$$

$$\phi_{ox} = V_{Gf}^{'} + \eta\left(\frac{z+t_{ox}}{\mathcal{T}_{sc}}\right)\left[V_{Gb}^{'} - V_{Gf}^{'} - \Psi_F\right]$$

$$+\frac{2}{\mathcal{T}_{sc}}\eta\sum_{n=1}^{\infty}\frac{f_{ox}^{(n)}(z)}{\alpha_n\Delta_n}F_n\left(V_{Gf}^{'}, V_{Gb}^{'}; y\right), \quad \text{... (25)}$$

and

$$\phi_{bo} = V_{Gb}^{'} + \eta\left(\frac{z-t_{si}-t_{box}}{\mathcal{T}_{sc}}\right)\left[V_{Gb}^{'} - V_{Gf}^{'} + \Psi_B\right]$$

$$+\frac{2}{\mathcal{T}_{sc}}\eta\sum_{n=1}^{\infty}\frac{f_{bo}^{(n)}(z)}{\alpha_n\Delta_n}F_n\left(V_{Gf}^{'}, V_{Gb}^{'}; y\right), \quad \text{... (26a)}$$

where

$$\mathrm{Er(z)} = \mathrm{erf}\left(\frac{z-\mu_p}{\sqrt{2}\sigma_p}\right) + \mathrm{erf}\left(\frac{\mu_p}{\sqrt{2}\sigma_p}\right),$$

$$\mathrm{Ex(z)} = \exp\left\{-\frac{1}{2}\left(\frac{z-\mu_p}{\sigma_p}\right)^2\right\} - \exp\left\{-\frac{1}{2}\left(\frac{\mu_p}{\sigma_p}\right)^2\right\},$$

$$\Psi_F = V_0\left\{\left(\frac{t_{si}+t_b-\mu_p}{\sqrt{2}\sigma_p}\right)\mathrm{Er}(t_{si}) + \frac{1}{\sqrt{\pi}}\mathrm{Ex}(t_{si})\right\},$$

$$\Psi_B = V_0\left\{\left(\frac{t_g+\mu_p}{\sqrt{2}\sigma_p}\right)\mathrm{Er}(t_{si}) - \frac{1}{\sqrt{\pi}}\mathrm{Ex}(t_{si})\right\},$$

$$V_0 = \frac{qD_0\sigma_P}{\epsilon_o\epsilon_{si}\sqrt{2}},$$

followed by

$$F_n(U,V;y) = \phi_{SD}^{(n)}(U,V)\frac{\cosh(\alpha_n y)}{\cosh(\alpha_n L/2)} + \frac{1}{2}V_D\zeta_n\frac{\sinh(\alpha_n y)}{\sinh(\alpha_n L/2)}, \quad \text{... (26b)}$$

$$\phi_{SD}^{(n)}(U,V) = \left(\phi_{SS}^{f} + \frac{1}{2}V_D - U\right)\chi_n^f + \left(\phi_{SS}^{b} + \frac{1}{2}V_D - V\right)\chi_n^b - S_n, \quad \text{... (26c)}$$

$$S_n = V_0\widehat{\Omega}_n + \frac{kT}{q}\left\{\frac{(t_{si}-\mu_p)t_b}{\sigma_p^2}\chi_n^b + \frac{t_g\mu_p}{\sigma_p^2}\chi_n^f - \frac{1+Q_n}{\sigma_p^2\alpha_n^2}\right\},$$

$$\widehat{\Omega}_n = \exp\left\{-\frac{1}{2}\left(\frac{\mu_p}{\sigma_P}\right)^2\right\}\left\{\frac{1}{\sqrt{2}\sigma_p\alpha_n}\omega_I\left(-\frac{\mu_p}{\sqrt{2}\sigma_p}, \frac{\alpha_n\sigma_p}{\sqrt{2}}\right) - \left(\frac{t_g}{\sqrt{2}\sigma_p}\right)\chi_n^f\omega_R\left(-\frac{\mu_p}{\sqrt{2}\sigma_p}, \frac{\alpha_n\sigma_p}{\sqrt{2}}\right)\right\}$$

$$+\exp\left\{-\frac{1}{2}\left(\frac{t_{si}-\mu_p}{\sigma_P}\right)^2\right\}\left\{\frac{Q_n}{\sqrt{2}\sigma_p\alpha_n}\omega_I\left(\frac{t_{si}-\mu_p}{\sqrt{2}\sigma_p}, \frac{\alpha_n\sigma_p}{\sqrt{2}}\right) + \left(\frac{t_b}{\sqrt{2}\sigma_p}\right)\chi_n^b\omega_R\left(\frac{t_{si}-\mu_p}{\sqrt{2}\sigma_p}, \frac{\alpha_n\sigma_p}{\sqrt{2}}\right)\right\},$$

$$\zeta_n = \chi_n^f + \chi_n^b,$$

$$\chi_n^f = \frac{\tan(\alpha_n t_{ox})}{\alpha_n t_{ox}},$$

$$\chi_n^b = Q_n\frac{\tan(\alpha_n t_{box})}{\alpha_n t_{box}}.$$

Here, $\omega_R(u,v)$ and $\omega_I(u,v)$ are the real and imaginary parts of the probability integral, $\omega(u+iv)$with complex argument, defined as[28]:

$$\omega(u+iv) = \exp\{(u+iv)^2\}\mathrm{erfc}(u+iv),$$

$$\omega(u+iv) = \omega_R(u,v) + i\omega_I(u,v).$$

The dummy parameters, U and V correspond to $V_{Gf}^{'}$ and $V_{Gb}^{'}$ respectively for Eqs. (24)-(26), these parameters will change accordingly in the other expressions that follow.

The explicit potential expressions in Eqs. (24)-(26), which correspond to their respective layers, are the superposition of two components: the first component represents the long-channel behavior, while the second, presented in series form, includes the short-channel effects. The series converges very quickly; only four terms of the series need to be summed to obtain reasonably accurate results. Therefore, we retain the series summation throughout the formalism of the threshold voltages, which are described in the following sections

2.3 Threshold voltages

In order to establish the threshold voltage formulae in various cases, we have followed the same procedure as reported in earlier publications[29-30] pertaining to SOI MOSFET's. To include the charge coupling effect of front and back interfaces in the threshold voltages of the device under study, we assume two virtual electrodes, each situated at the minimum positions of the respective front and back surface potentials[31-33]. Therefore, considering Eq. (24), the minimum surface potentials at the virtual electrodes are defined as:

$$\phi_s^f = \phi_{si}(y_m, 0), \qquad \text{... (27)}$$

the front surface potential, ϕ_s^f, and that, ϕ_s^b, at back interface is

$$\phi_s^b = \phi_{si}(y_m', t_{si}). \qquad \text{... (28)}$$

The virtual electrode positions y_m and y_m' can be determined by setting

$$\frac{\partial \phi_{si}}{\partial y}(y = y_m, 0) = \frac{\partial \phi_{si}}{\partial y}(y = y_m', t_{si}) = 0, \qquad \text{... (29)}$$

for front and back interfaces respectively. The electrode positions y_m and y_m' cannot be the same unless s$\phi_s^f = \phi_s^b$ or $V_D = 0$. In the present case, these cannot be formulated explicitly. Instead, we have numerically calculated these values using the Newton-Raphson method. Approximately 10 to 12 iterations in this method yield fairly accurate results, while the overall calculation time is minimal.

In the SOI MOSFET, we assume that the silicon film is very thin, so that the complete depletion of the film can occur. As a result, both the front and back gates are coupled, rendering the dependence of each gate on the condition of the other. In order to analyze these dependences, we formulate front and back gate biases that include the charge coupling effects in terms of front and back surface potentials. Thus, the front gate voltage, derived with the help of Eqs. (27), (28) and (24), is given by:

$$V_{Gf} = V_{Gf}^0 + \Delta V_{Gf}. \qquad \text{... (30)}$$

Here, V_{Gf}^0 is the front gate voltage, which remains unaffected by short channel length expressed by

$$V_{Gf}^0 = V_{FB}^f + V_{Gf}^{0\prime},$$

where

$$V_{Gf}^{0\prime} = \left(1 + \frac{t_g}{t_{si}}\right)\phi_s^f - \left(\frac{t_g}{t_{si}}\right)\phi_s^b + \left(\frac{t_g}{t_{si}}\right)V_0 \times \left[\left(\frac{t_{si} - \mu_p}{\sqrt{2}\sigma_p}\right)\mathrm{Er}(t_{si}) + \frac{1}{\sqrt{\pi}}\mathrm{Ex}(t_{si})\right]. \qquad \text{... (30a)}$$

ΔV_{Gf} is the front gate voltage shift due to short channel effect which is written as:

$$\Delta V_{Gf} = \frac{\left(\frac{t_g}{t_{si}}\right)\Gamma_b\left(V_{Gf}^{0\prime}, V_{Gb}^{0\prime}\right) - \left(1 + \frac{t_g}{t_{si}}\right)\Gamma_f\left(V_{Gf}^{0\prime}, V_{Gb}^{0\prime}\right)}{1 - [\Upsilon_f + \Upsilon_b]}, \qquad \text{... (30b)}$$

which includes

$$\Gamma_f\left(V_{Gf}^{0\prime}, V_{Gb}^{0\prime}\right) = \frac{2t_g}{\mathcal{T}_{sc}}\sum_{n=1}^{\infty}\left(\frac{\chi_n^f}{\Delta_n}\right)F_n\left(V_{Gf}^{0\prime}, V_{Gb}^{0\prime}; y_m\right),$$

$$\Gamma_b\left(V_{Gf}^{0\prime}, V_{Gb}^{0\prime}\right) = \frac{2t_b}{\mathcal{T}_{sc}}\sum_{n=1}^{\infty}\left(\frac{\chi_n^b}{\Delta_n}\right)F_n\left(V_{Gf}^{0\prime}, V_{Gb}^{0\prime}; y_m'\right),$$

$$\Upsilon_f = \frac{2t_g}{\mathcal{T}_{sc}}\sum_{n=1}^{\infty}\frac{\chi_n^f}{\Delta_n}\left\{\left(1 + \frac{t_g}{t_{si}}\right)\chi_n^f - \frac{t_b}{t_{si}}\chi_n^b\right\}\frac{\cosh(\alpha_n y_m)}{\cosh(\alpha_n L/2)},$$

$$\Upsilon_b = \frac{2t_b}{\mathcal{T}_{sc}}\sum_{n=1}^{\infty}\frac{\chi_n^b}{\Delta_n}\left\{\left(1 + \frac{t_b}{t_{si}}\right)\chi_n^b - \frac{t_g}{t_{si}}\chi_n^f\right\}\frac{\cosh(\alpha_n y_m')}{\cosh(\alpha_n L/2)}.$$

The front gate bias shift, ΔV_{Gf}, shown by Eq. (30b), comprises the effect of short channel length, scaling down of which induces ΔV_{Gf} to increase in negative direction, whereby the front gate bias, V_{Gf}, degrades. This is evidenced by analyzing the numerator and denominator of Eq. (30b). Besides, ΔV_{Gf} also depends on drain voltage, V_D, which introduces barrier lowering effect causing thereby further degradation of V_{Gf}. From these remarks, it is clear that the front interface of short channel device can turn on with reduced value of V_{Gf} in comparison with that applied on long channel device. Likewise, the back gate bias derived as follows:

$$V_{Gb} = V_{Gb}^0 + \Delta V_{Gb}, \qquad \text{... (31)}$$

where

$$V_{Gb}^o = V_{FB}^b + V_{Gb}^{0\prime},$$

with

$$V_{Gb}^{0\prime} = \left(1+\frac{t_b}{t_{si}}\right)\phi_s^b - \left(\frac{t_b}{t_{si}}\right)\phi_s^f + \left(\frac{t_b}{t_{si}}\right)V_0 \times \left[\left(\frac{\mu_p}{\sqrt{2}\sigma_p}\right)\mathrm{Er}(t_{si}) - \frac{1}{\sqrt{\pi}}\mathrm{Ex}(t_{si})\right]. \quad \text{... (31a)}$$

The back gate voltage shift, ΔV_{Gb}, due to short channel effect is given as

$$\Delta V_{Gb} = \frac{\left(\frac{t_b}{t_{si}}\right)\Gamma_f\left(V_{Gf}^{0\prime},V_{Gb}^{0\prime}\right) - \left(1+\frac{t_b}{t_{si}}\right)\Gamma_b\left(V_{Gf}^{0\prime},V_{Gb}^{0\prime}\right)}{1-[\Upsilon_f+\Upsilon_b]}. \quad \text{... (31b)}$$

From Eq. (31b) it is clear that back gate bias shift, ΔV_{Gb}, is apparently different from ΔV_{Gf}, obtained in Eq. (30b). This expression can also be explained in the same way as Eq. (30b). Equation (31) along with Eqs. (31a) and (31b) is useful in deciding back gate bias for accumulation or inversion mode of back gate interface for the study of front gate threshold voltage. On the other hand, Eq. (30) along with Eqs. (30a) and (30b) is important to achieve particular mode of operation of front gate interface while analyzing back gate threshold voltage. Therefore, Eqs. (30) and (31) are the key relations, which describe the front and back interface coupling of FD-SOI MOSFET in terms of their respective surface potential at the virtual electrodes. Combining those, leads to a description of both front and back gate threshold voltages, which are given as follows.

2.3.1 Front threshold voltage

For threshold condition of the front interface i.e. for $\phi_s^f = 2\psi_B^f$ (where ψ_B^f is the Fermi potential at front interface), if the back interface of SOI MOSFET is in accumulation, ϕ_s^b is pinned down to zero for the fully-depleted transistor or body bias, V_B, applied to fully deplete silicon film for partially depleted one. In this case, as per Eq. (30), (30a) and (30b), the front gate biasing parameters get converted to $V_{Gf} \equiv V_{Tf}^A$, $V_{Gf}^{0\prime} \equiv V_{Tf}^{\mathrm{A}0\prime}$ and $\Delta V_{Gf} \equiv \Delta V_{Tf}^A$ i.e. the front threshold voltages at back interface accumulation. The corresponding back gate biases under the similar condition can be found out by making use of Eq. (31), (31a) and (31b), which are $V_{Gb} \equiv V_{Gb}^A$, $V_{Gb}^{0\prime} \equiv V_{Gb}^{\mathrm{A}0\prime}$ and $\Delta V_{Gb} \equiv \Delta V_{Gb}^A$. Under such a situation, the threshold voltage,V_{Tf}^A, is the maximum and it becomes independent of back gate bias, V_{Gb}.

When the back interface is in inversion i.e. $\phi_s^b = 2\psi_B^b$ (here ψ_B^b is the Fermi potential at back interface), then Eq. (30), (30a) and (30b) take the form as $V_{Gf} \equiv V_{Tf}^I$, $V_{Gf}^{0\prime} \equiv V_{Tf}^{I0\prime}$ and $\Delta V_{Gf} \equiv \Delta V_{Tf}^I$ respectively referred to as threshold voltages at back interface inversion. Similarly the back gate bias parameters at this state of back interface inversion are modified versions of Eq. (31), (31a) and (31b) those are: $V_{Gb} \equiv V_{Gb}^I$, $V_{Gb}^{0\prime} \equiv V_{Gb}^{I0\prime}$ and $\Delta V_{Gb} \equiv \Delta V_{Gb}^I$ respectively, if we put $\phi_s^f = 2\psi_B^f$ and $\phi_s^b = 2\psi_B^b$. In this case, inversion threshold voltage, V_{Tf}^I, goes down considerably low and becomes independent of back gate bias. Thus, the onsets of back interface accumulation ($\phi_s^b = 0$) and inversion ($\phi_s^b = 2\psi_B^b$) set the range of back gate bias, V_{Gb}.

In the case where the back interface is in depletion, the depletion threshold voltage, V_{Tf}^D, varies with V_{Gb}, because, ϕ_s^b strongly depends on the back gate bias; its value ranges about zero to $2\psi_B^b$. Accordingly, V_{Gb}, lies within the range, $V_{Gb}^A < V_{Gb} < V_{Gb}^I$. Beyond this range of V_{Gb}, ϕ_s^b is invariant, which in turn ϕ_s^b shields the effect of back gate voltage in the real devices. Therefore to formulate depletion threshold voltage, we consider Eq. (27) and apply the strong inversion criterion ($\phi_s^f = 2\psi_B^f$) at the front interface. The Eq. (27) with the help of Eq. (24), after some arrangements, gives the expression of front gate voltage, V_{Gf}, and then we replace V_{Gf} by V_{Tf}^D, to yield

$$V_{Tf}^D = V_{Tf}^{D0} + \Delta V_{Tf}^D, \quad \text{... (32)}$$

where V_{Tf}^{D0} is the long channel front threshold voltage defined as:

$V_{Tf}^{D0} = V_{Tf}^{D0\prime} + V_{FB}^f$, which includes

$$V_{Tf}^{D0\prime} = 2\psi_B^f + \left[2\psi_B^f - V_{Gb}^{\prime} + \Psi_F\right]\left(\frac{t_g}{t_{si}+t_b}\right). \quad \text{... (32a)}$$

The front threshold voltage shift due to short channel length is given as

$$\Delta V_{Tf}^D = -\frac{\Gamma_f\left(V_{Tf}^{D0\prime},V_{Gb}^{\prime}\right)}{\varrho_f - \xi_f}, \quad \text{(32b)}$$

where

$$\varrho_f = (t_{si} + t_b)/\mathcal{T}_{sc},$$

$$\xi_f = \frac{2t_g}{\mathcal{T}_{sc}}\sum_{n=1}^{\infty}\left(\frac{\chi_n^f}{\Delta_n}\right)\chi_n^f\frac{\cosh(\alpha_n y_m)}{\cosh(\alpha_n L/2)}.$$

The depletion threshold voltage expressed by Eq. (32) along with (32a) and (32b) has combined effects of back gate bias,V_{Gb}, drain voltage, V_D, and

short channel length besides effect of annealing through, σ_p.

2.3.2 Back threshold voltage

If the back interface turns on prior to front interface, then we apply strong inversion criterion ($\phi_s^b = 2\psi_B^b$) at the back interface. In this case, V_{Gf} is treated as a controlling parameter for back depletion threshold voltage, V_{Tb}^D. The respective back gate threshold voltages, V_{Tb}^A and V_{Tb}^I, corresponding to their onsets of front interface accumulation ($\phi_s^f = 0$) and inversion ($\phi_s^f = 2\psi_B^f$) can be obtained by making use of Eq. (31). Similarly the respective front gate voltages, V_{Gf}^A and V_{Gf}^I, pertaining to their onsets can be deduced from Eq. (30). Accordingly the range, $V_{Gf}^A < V_{Gf} < V_{Gf}^I$ of V_{Gf}, about these onsets can be decided. Now, we apply the strong inversion criterion on back interface and solve Eq. (28) with the help of Eq. (24) for back gate voltage,V_{Gb}, and then we replace it by V_{Tb}^D to yield

$$V_{Tb}^D = V_{Tb}^{D0} + \Delta V_{Tb}^D, \quad \text{... (33)}$$

where V_{Tb}^{D0} is the long channel back threshold voltage which is written as

$$V_{Tb}^{D0} = V_{Tb}^{D0'} + V_{FB}^b,$$

followed by

$$V_{Tb}^{D0'} = 2\psi_B^b + \left[2\psi_B^b - V_{Gf}' + \Psi_B\right]\left(\frac{t_b}{t_{si}+t_g}\right), \quad \text{... (33a)}$$

and the back threshold voltage shift, ΔV_{Tb}^D, due short channel effect, is given by

$$\Delta V_{Tb}^D = -\frac{\Gamma_b\left(V_{Gf}', V_{Tb}^{D0'}\right)}{\varrho_b - \xi_b}, \quad \text{... (33b)}$$

$$\varrho_b = \left(t_{si} + t_g\right)/\mathcal{T}_{sc},$$

$$\xi_b = \frac{2t_b}{\mathcal{T}_{sc}} \sum_{n=1}^{\infty} \left(\frac{\chi_n^b}{\Delta_n}\right) \chi_n^b \frac{\cosh(\alpha_n y_m')}{\cosh(\alpha_n L/2)}.$$

The back gate threshold voltage expression given in Eq. (33) along with (33a) and (33b) consists of the effects of V_{Gf}, $V_D$and channel length. Besides, it also includes annealing effect through σ_p as Eq. (33) has.

As mentioned earlier, the present formalism is based on the assumption that there are negligible mobile charges in depleted SOI film of the transistor. If, we analyse threshold voltage expression given as Eq. (32) along with (32a) and (32b), the front depletion threshold voltage, V_{Tf}^D, decreases linearly as we increase V_{Gb} from V_{Gb}^A to V_{Gb}^I irrespective of different values of channel length, L, but, slope of such variation depends upon L(see Fig. 2). Beyond this range of back gate bias, i.e. for $V_{Gb} < V_{Gb}^A$ and for $V_{Gb} > V_{Gb}^I$, the threshold voltage V_{Tf}^D saturates and attains the respective values V_{Tf}^A and V_{Tf}^I. Such variation of V_{Tf}^D with V_{Gb} causes discontinuities at the onset points of back interface accumulation ($\phi_s^b = 0$) and inversion ($\phi_s^b = 2\psi_B^b$) which are unrealistic, because, transitions from one space charge to another are not abrupt[34-35] as we implicitly assumed in the present analysis. Actually, ϕ_s^b corresponding to their accumulation and inversion differs from zero and $2\psi_B^b$ by few thermal voltages (rkT/q where, $r\sim5$) depending upon the degree of accumulation and inversion[29-30]. However, these differences are much smaller than the variation of ϕ_s^b between accumulation to inversion and, therefore, do notaffectV_{Tf}^D variation withV_{Gb}. This is in accordance with the fact that the effective width of accumulation or inversion charges across which voltage rkT/q isdropped, are much smaller than film thickness, t_{si}, which was assumed in solving Poisson's Eq. (2), where we have ignored charge carriers. Likewise, the ignorance of accumulation or inversion charges in case of $V_{Tb}^D(V_{Gf})$ variations and in its respective values V_{Tb}^A and V_{Tb}^I corresponding to their onsets of front interface accumulation ($\phi_s^f = 0$) and inversion ($\phi_s^f = 2\psi_B^f$) is also justified.

3 Results and Discussion

In this section the results of potential distributions and threshold voltages obtained from theoretical

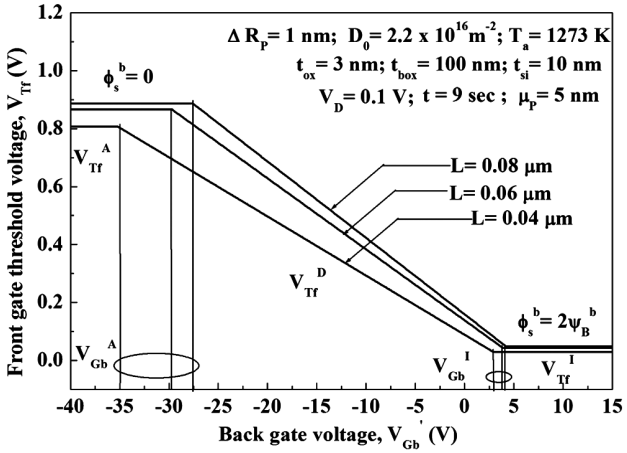

Fig. 2 — Front gate threshold voltage variations with back gate bias for different values of channel length

model are presented and compared with ATLAS data[36]. Fig. 3 shows the distributions of front and back surface potentials along the channel of the device, calculated with the help of Eq. (24) at $z = 0$ and $z = t_{si}$ respectively for different values of channel length, whereas, Fig. 4 displays the calculated results of potential variations along the thickness of SOI film at $y = 0$. Both the plots show excellent matching of the model results with those of ATLAS software even for the smallest value of channel length used in the calculations.

Figure 5 exhibits the annealing effects on the front and back gate depletion threshold voltages calculated with the help of Eqs. (32) and (33) respectively. As annealing time increases, both the threshold voltages decrease in their magnitudes. At the same time, the short channel effect becomes less pronounced as the doping concentration changes within the channel[33, 37]

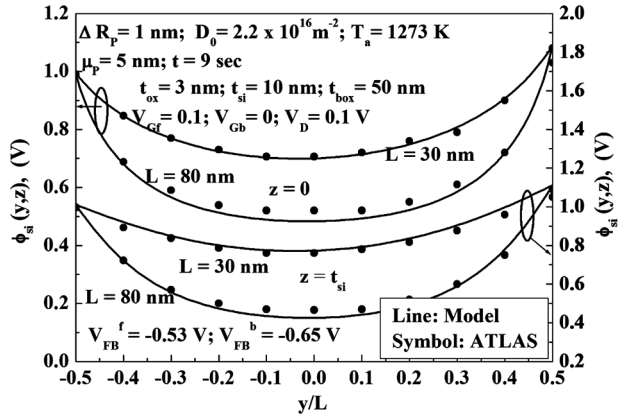

Fig. 3 — Surface potential distribution at both front and back interfaces of SOI MOSFET for different values of channel length, *L* and their comparison with ATLAS data

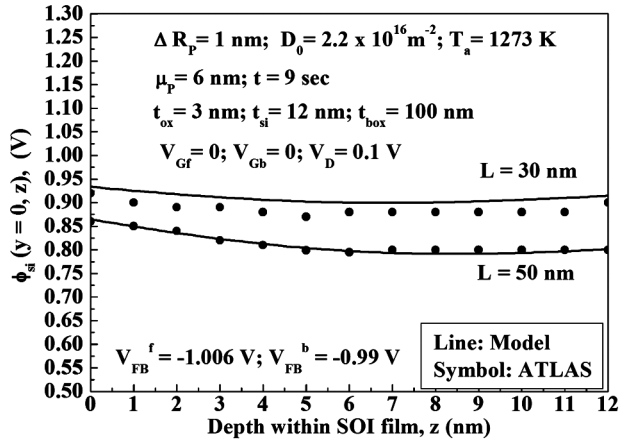

Fig. 4 — Vertical potential distribution within the SOI film for different channel length of SOI MOSFET and their comparison with ATLAS results

due to annealing time. This can be further explained as follows: During the implantation, if energy of incident boron ions is greater than the binding energy of matrix atom (Si), the former displace the host atoms by transferring their energy through nuclear processes, thus generating point defects such as vacancies and silicon self-interstitials thereby creating defect rich region at about ion projection range, R_p. The dopant atoms accumulate at this zone and are distributed following the Gaussian function given in Eq. (4).

During thermal treatment, implanted atoms undergo exchange through the aforementioned point defects. When boron substitutional atoms approach the vacancies, both are annihilated, thereby creating a defect-free zone. At the same time, the remaining dopant atoms that survive as interstitials diffuse away from the maximum stopping power zone, thus reducing the peak concentration. Such a redistribution of dopant atom follows Eq. (5). The exchange process of impurity atoms via point defects continues for a longer duration for further increase in annealing time. As a result, the boron out diffusion along with damage repair in silicon continues leading to the further reduction of concentration (Fig. 1b). Such a decrease of impurity concentration leads to the reduction of threshold voltages as the annealing time increases. Zhang *et al*., also demonstrated the reduction of threshold voltage with increasing doping concentration[16], thereby affirming the efficacy of this model.

The effects of silicon film thickness on the depletion threshold voltages of the front and back gates, calculated using Eqs. (32) and (33), are shown in Fig. 6 with an annealing time is 9 seconds. The higher film thickness,t_{si}, obviously causes the

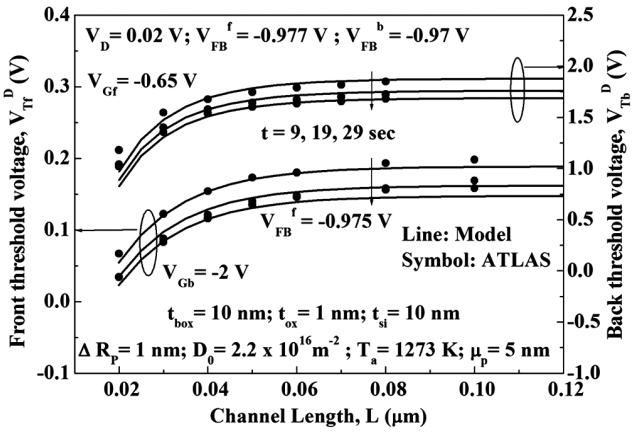

Fig. 5 — Front- and back-gate threshold voltage variations with the channel lengths considering annealing time, t, as a parameter andeir comparison with ATLAS results

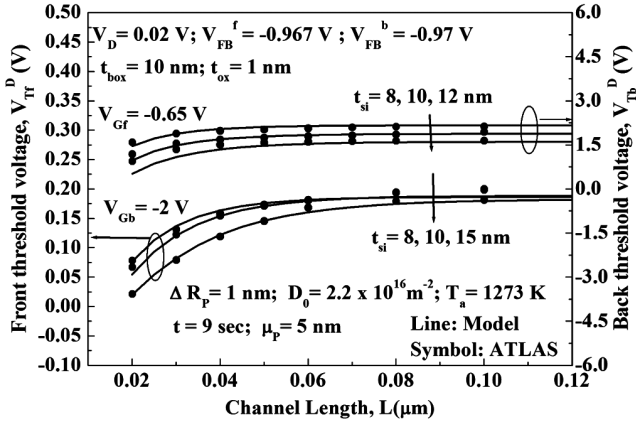

Fig. 6 — Front- and back-gate threshold voltage variations with the channel length for different values of SOI film thicknesses and their comparison with ATLAS results

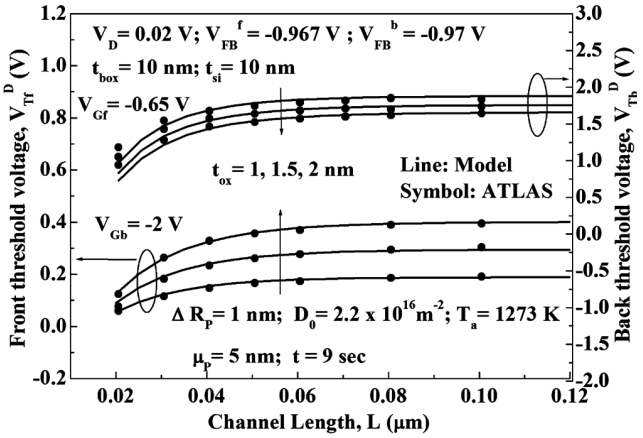

Fig. 7 — Front threshold voltage and back threshold voltage variation with the channel length, calculated from the present model and ATLAS simulator, at different values of thickness of front oxide

increase in magnitudes of both the threshold voltages and simultaneously enhancement of short channel effects. The variations of front and back gate threshold voltages with channel length for different values of front oxide thickness (Fig. 7) also show the increasing tendency in their magnitudes and more pronounced short channel effects at the same time, as oxide thickness increases.

4 Conclusion

The study introduces novel analytical models that provide explicit closed-form expressions for both the front and back gate threshold voltages of FD-SOI MOSFETs. This represents a substantial contribution to the understanding of device behavior in relation to the effects introduced by retrograde doping. The exact solutions of 2-D Laplace/Poisson's equations with annealed non-uniform channel doping have been obtained for potential relations in the three-layer structure of SOI MOSFET by leveraging a new Green's function approach. The new Green's functions for each layer have been established by considering realistic boundary conditions at the interfaces, rendering the Green's function of each layer dependent on the conditions at the others. Based on presently derived potential relations, the established closed form expressions of the front and back gate threshold voltages comprise the annealing effect of channel doping and the effect of drain induced barrier lowering; besides, front and back gate charge coupling arise due to the depleted SOI film of the transistor. Long-time thermal treatment of the channel implant facilitates the redistribution of dopant atoms via diffusion mechanism, thereby decreasing the doping concentration. As a consequence, both front and back gate threshold voltages decrease in their magnitudes, and concurrently the short channel effects become less pronounced. Thus, by annealing the implanted channel for an appropriate time and temperature, the threshold voltages can be adjusted, and the short-channel effects can be minimized. Hence the model predicts that the channel length of the present device can also be scaled down up to nanometer ranges without significant degradation of the threshold voltages. Additionally, the operational modes of the device can be determined by formulating the corresponding back and front gate bias voltages. The study provides a framework for determining the operational modes of the device. This is a key for practical applications, as it gives engineers and researchers insights into optimizing device performance under various operating conditions. The results of the present models and those of ATLAS software show excellent matching.

Acknowledgements

The authors would like to thank the Director, BK BIET-Pilani and the Director, CSIR CEERI, Pilani for their invaluable support, constant motivations and guidance throughout this research. We appreciate the resources and opportunities provided, which have significantly contributed to the completion of this project.

Appendix

Here we describe the procedure to derive the Green's functions, which have the combined effect of all the three zones (front oxide, SOI film and back

oxide). In this approach we first deal with the set of differential Eq. (18) to arrive at the explicit expressions of Greens functions pertaining to silicon layer, other sets, Eq. (19) and Eq. (20), of differential equations can be tackled accordingly to achieve the solutions of Green's functions related to respective front and back oxide layers. Let us assume that the solutions of Eq. (18) are

$$G_{ox} = A_{ox}\cos(\alpha z) + B_{ox}\sin(\alpha z), \quad (A-1)$$
$$G_{si} = A_{si}\cos(\alpha z) + B_{si}\sin(\alpha z), \quad (A-2)$$
$$G_{bo} = A_{bo}\cos(\alpha z) + B_{bo}\sin(\alpha z), \quad (A-3)$$

For brevity, we have dropped the arguments of Green's functions. The application of homogeneous conditions of boundary values given in Eqs. (6), (13) and interface boundary conditions in Eqs. (14)-(17) in Eqs.(A-1)-(A-3), yields,

$$G_{ox} = \eta\sum_{n=1}^{\infty} B_{si}^{(n)} f_{ox}^{(n)}(z), \quad (A-4)$$

$$G_{si} = \sum_{n=1}^{\infty} B_{si}^{(n)} f_{si}^{(n)}(z), \quad (A-5)$$

$$G_{bo} = \eta\sum_{n=1}^{\infty} B_{si}^{(n)} f_{bo}^{(n)}(z), \quad (A-6),$$

The Eigen functions representing respective layers are written as:

$$f_{si}^{(n)}(z) = \sin(\alpha_n z) + \eta\tan(\alpha_n t_{ox})\cos(\alpha_n z), \quad (A-7)$$

$$f_{ox}^{(n)}(z) = \frac{\sin\alpha_n\,(z + t_{ox})}{\cos(\alpha_n t_{ox})}, \quad (A-8)$$

$$f_{bo}^{(n)}(z) = Q_n\frac{\sin\alpha_n(t_{si} + t_{box} - z)}{\cos\,(\alpha_n t_{box})}, \quad (A-9)$$

where

$$Q_n = \eta\,\tan(\alpha_n t_{ox})\sin(\alpha_n t_{si}) - \cos(\alpha_n t_{si}), (A-10)$$

and Eigen values α_n are the non-zero positive roots of the equation,

$$\tan(\alpha_n t_{si}) = \frac{\eta\{\tan(\alpha_n t_{box}) + \tan(\alpha_n t_{ox})\}}{\eta^2\tan(\alpha_n t_{box})\tan(\alpha_n t_{ox}) - 1}. \quad (A-11)$$

Here n is the integer varying as, 1, 2, 3, ..., ∞.The Eq. (A-11) is identical to that derived[24] with different approach.

It may be noted that the series coefficients, $B_{si}^{(n)}$, are common in all the series given in Eqs.(A-4)-(A-6). Through these coefficients, the Green's function includes the combined effect of all the regions. Besides, the series (A-4)-(A-6) are orthogonal in nature in the range, $-t_{ox} \le z \le t_{si} + t_{box}$. Now, we substitute Eqs.(A-4)-(A-6) in respective differential equations of Eq. (18) and then take their Fourier series transform, which results in the single differential equation in one-dimensional form as:

$$\frac{\partial^2 B_{si}^{(n)}}{\partial y^2} - \alpha_n^2 B_{si}^{(n)} = \frac{2f_{si}^{(n)}(z')}{\mathcal{T}_{sc}\Delta_n}\delta(y - y'). \quad (A-12)$$

The Eigen function appeared in Eq. (A-12) corresponds to silicon layer because the source point of Green's function is located in that layer. It is worth mentioning here that the series, (A-4)-(A-6), can also be used for transformation purpose of sets Eqs. (19) and (20). The series parameterΔ_n is defined as:

$$\Delta_n = \frac{t_b}{\mathcal{T}_{\rm sc}}Q_n^2\sec^2(\alpha_n t_{box}) + \frac{t_g}{\mathcal{T}_{sc}}\sec^2(\alpha_n t_{ox}) + \frac{t_{si}}{\mathcal{T}_{\rm sc}}\{1 + \eta^2\tan^2(\alpha_n t_{ox})\},$$

where

$$t_g = \eta t_{ox};\ \ t_b = \eta t_{box},$$

and the total scaled thickness of three-layer structure is

$$\mathcal{T}_{sc} = t_g + t_{si} + t_b$$

The Eq. (A-12) can easily be solved in the usual way[27]. The boundary values for this purpose are deduced by assuming homogeneous conditions of respective source and drain end ones in Eqs. (7)-(9) and Eqs. (10)-(12), which yield, $B_{si}^{(n)}(y = \pm L/2) = 0$. Additionally, we also apply the usual discontinuity of Green's function by integrating Eq. (A-12) once about the source position i.e.

$$\frac{\partial B_{si}^{(n)+}}{\partial y}(y = y') - \frac{\partial B_{si}^{(n)-}}{\partial y}(y = y') = \frac{2f_{si}^{(n)}(z')}{\mathcal{T}_{sc}\Delta_n},$$

along with their equality at the source point given by

$$B_{si}^{(n)+}(y = y') = B_{si}^{(n)-}(y = y').$$

Thus, the complete Green's function solutions in explicit form are shown by Eq. (23).

References

1 Das A, Rewari S & Kanaujia B K & Gupta R S, *Silicon,* 14 (2022) 5133.
2 Goyal P, Srivastava G, Madan J, Pandey R & Gupta R S, *Mater Sci Eng,* 304 (2024) 117356.
3 Mann R, Rewari S, Sharma S & Gupta R S, *Semicond Sci Technol,* 3 (2023) 035012.
4 Chakraborty A & Sarkar A, *J Comput Electron,* 16 (2017) 556.
5 Sharma S, Nath V, Deswal S S & Gupta R S, *Microelctronics J,* 129 (2022) 05599.
6 Das A, Kanaujia B K, Nath V, Rewari S & Gupta R S, *IEEE 17th India Counc Int Conf INDICON,* (2020) 1.
7 Hsiao T C, Liu P & Woo J C S, *IEEE Trans Electron Dev***,** ED-45 (1998) 1092.
8 Khanna V K, *Integrated Nanoelectronics,* (Springer, New Delhi) (2016) 73. https://doi.org/10.1007/978-81-322-3625-2_5
9 Xu J & Cheng MC, *Proc. 3rd IEEE Int Caracas Conf Dev Circuits Syst*, D29 (2003) 1-5.
10 Yu F X, Cheng M C & Xu J, *Proc Int Semicond Device Res Sym*, (2001) 613.
11 Sze S M, Physics of semiconductor devices, (Wiley Eastern Limited, New Delhi) 2nd Edn, (1983) 71.
12 Suzuki K & Kataoka Y, *et al*., *IEEE Trans Electron Dev,* ED-54 (2007) 262.
13 Madadi *et al*, *Silicon,* 13 (2021) 645.
14 Huang H, *et al*., *IEEE Trans Nuclear Sci,* 65 (2018) 679.
15 Pandey P, *et al*., *IEEE Trans Electron Dev,* ED-51 (2004) 246.
16 Zhang G, *et al*., *IEEE Trans Electron Dev*, ED-55 (2008) 803.
17 Lin P S, *et al., IEEE Trans Electron Dev*, ED-34 (1987) 1947.
18 Chin SP, *et al.,IEEE Trans Electron Dev,* ED-39 (1992) 1928.
19 Guo J Y, *et al., IEEE Trans Electron Dev*, ED-40 (1993) 1653.
20 Meer H V, *et al., IEEE Trans Electron Dev,* ED-48 (2001) 2292.
21 Tanaka S*et al., IEEE Trans Electron Dev,* ED-33 (1986) 743.
22 Ghoshtagore R N, *Phys Rev*, B3 (1971) 2507.
23 Goyal P, Srivastava G, Madan J, Pandey R & Gupta R S, *Phys Scr,* 99 (2024) 015008.
24 Das A, *et al*., *Int J Numer Model*, 36 (2023) e3106.
25 Yadav S, Das A & Rewari S, *ECS J Solid State Sci Technol*, 13 (2024) 047001.
26 Inglesfield J E, *J Phys C: Solid State Phys***,** 4 (1971) L14.
27 Morse P M & Feshbach H, *Methods of theoretical physics,* Part-I (McGraw-Hill Book Comp, New York),(1953) 791.
28 Magnus W, Oberhettinger F & Soni R P, *Formulas and theorems for the special functions of mathematical physics,* (Springer-Verlag, New York Inc), 1996, 52.
29 Lim H K & Fossum J G, *IEEE Trans Electron Dev*, ED-30 (1983) 1244.
30 Meel K, *et al., Solid-State Electron,* 62 (2011) 174.
31 Das A *et al., Phys Scr,* 98 (2023) 074005.
32 Das A *et al., J Comput Electron,* 22 (2023) 742.
33 Das A *et al., Phys Scr,* 98 (2023) 115013.
34 Kamgar A, *et al., IEEE Trans Electron Dev,* ED-39 (1992) 640.
35 Burignat S, *et al., Solid-State Electron,* 54 (2010) 213.
36 ATLAS User's Manual: *Silvaco Data System Inc*, Version 5.15.31.C, (2009).
37 Das A, *et al., Microelectronics J,* 138 (2023) 105832.